



HAL
open science

Room-Temperature Epitaxial Growth of Zn-Doped Iron Oxide Films on c-, a-, and r-Cut Sapphire Substrates

Valérie Demange, Xavier Portier, Sophie Ollivier, Mathieu Pasturel, Thierry Roisnel, Maryline Guilloux-Viry, Christian Hebert, Magdalena Nistor, Christophe Cachoncinlle, Eric Millon, et al.

► To cite this version:

Valérie Demange, Xavier Portier, Sophie Ollivier, Mathieu Pasturel, Thierry Roisnel, et al.. Room-Temperature Epitaxial Growth of Zn-Doped Iron Oxide Films on c-, a-, and r-Cut Sapphire Substrates. *Crystal Growth & Design*, 2023, 23 (12), pp.8534-8543. 10.1021/acs.cgd.3c00404 . hal-04350858

HAL Id: hal-04350858

<https://hal.science/hal-04350858v1>

Submitted on 2 Feb 2024

HAL is a multi-disciplinary open access archive for the deposit and dissemination of scientific research documents, whether they are published or not. The documents may come from teaching and research institutions in France or abroad, or from public or private research centers.

L'archive ouverte pluridisciplinaire **HAL**, est destinée au dépôt et à la diffusion de documents scientifiques de niveau recherche, publiés ou non, émanant des établissements d'enseignement et de recherche français ou étrangers, des laboratoires publics ou privés.

This document is confidential and is proprietary to the American Chemical Society and its authors. Do not copy or disclose without written permission. If you have received this item in error, notify the sender and delete all copies.

Room temperature epitaxial growth of Zn-doped iron oxide films on c-, a- and r-cut sapphire substrates

Journal:	<i>Crystal Growth & Design</i>
Manuscript ID	cg-2023-004046.R3
Manuscript Type:	Article
Date Submitted by the Author:	n/a
Complete List of Authors:	Demange, Valérie; Université de Rennes, Institut des Sciences Chimiques de Rennes Portier, Xavier; Université de Caen Normandie, Centre de recherche sur les Ions, les MATériaux et la Photonique (CIMAP), CEA/UMR CNRS 6252 Ollivier, Sophie; Université de Rennes, Institut des Sciences Chimiques de Rennes Pasturel, Mathieu; Université de Rennes, Institut des Sciences Chimiques de Rennes, UMR CNRS 6226 Roisnel, Thierry; Université de Rennes, Institut des Sciences Chimiques de Rennes Guilloux-Viry, Maryline; ISCR Hebert, Christian; Sorbonne Université, Institut des NanoSciences de Paris (INSP), CNRS UMR 7588 NISTOR, Magdalena; National Institute for Laser Plasma and Radiation Physics, Plasma Physics and Nuclear Fusion Laboratory (L22) Cachoncinlle, Christophe; Université d'Orléans, GREMI UMR 7344 Millon, Eric; Université d'Orléans, GREMI UMR 7344 Perrière, Jacques; Sorbonne Université, Institut des NanoSciences de Paris (INSP), CNRS UMR 7588

SCHOLARONE™
Manuscripts

1
2
3
4
5
6
7
8
9
10
11
12
13
14
15
16
17
18
19
20
21
22
23
24
25
26
27
28
29
30
31
32
33
34
35
36
37
38
39
40
41
42
43
44
45
46
47
48
49
50
51
52
53
54
55
56
57
58
59
60

Room temperature epitaxial growth of Zn-doped iron oxide films on c-, a- and r-cut sapphire substrates

Valérie Demange^{1,}, Xavier Portier², Sophie Ollivier¹, Mathieu Pasturel¹, Thierry Roisnel¹,
Maryline Guilloux-Viry¹, Christian Hebert³, Magdalena Nistor⁴, Christophe Cachoncinlle⁵, Eric
Millon⁵, Jacques Perriere³*

¹ Univ Rennes, CNRS, ISCR – UMR 6226, ScanMAT – UAR 2025, F-35000 Rennes, France

² Centre de recherche sur les Ions, les MATériaux et la Photonique (CIMAP), CEA/UMR CNRS
6252, Normandie Université, ENSICAEN, 14050 Caen Cedex, France

³ Institut des NanoSciences de Paris (INSP), CNRS UMR 7588 Sorbonne Université, 4 Place
Jussieu, Paris Cedex 05 75252, France

⁴ National Institute for Lasers, Plasma and Radiation Physics (NILPRP), PO Box MG-36,
077125 Magurele-Bucharest, Romania

⁵ GREMI UMR 7344 CNRS-Université d'Orléans, 45067 Orléans Cedex 2, France

KEYWORDS: Oxide thin film. Room-temperature epitaxy. Van der Waals Epitaxy.
Graphoepitaxy. Pulsed laser deposition.

1
2
3
4 ABSTRACT. The room temperature growth of zinc-doped iron oxide films (Zn:FeO_x) was studied
5
6 on c-cut, a-cut and r-cut sapphire substrates using the pulsed-laser deposition method. Rutherford
7
8 backscattering spectrometry, X-ray diffraction analysis, pole figure measurements and
9
10 transmission electron microscopy were used to determine the nature of the oxide phases (wüstite
11
12 and/or spinel) present in the films, their precise texture and in-plane epitaxial relationships between
13
14 films and substrates. On c-cut sapphire, both wüstite and spinel phases were present with a (111)
15
16 texture. The wüstite phase was mainly found at the film-substrate interface, while the spinel was
17
18 observed in the upper part of the film. On the a-cut and r-cut substrates, the main phase observed
19
20 was the wüstite, with a very small spinel contribution. The (111) and (100) wüstite textures were
21
22 obtained on the a-cut and r-cut substrates, respectively. The in-plane epitaxial relationships
23
24 between the Zn doped iron oxide phases and the substrates were deduced from transmission
25
26 electron spectroscopy observations and pole figure measurements. The possible mechanisms of
27
28 the room temperature epitaxial growth of the oxide films on r-cut and a-cut sapphire substrates are
29
30 presented and discussed.
31
32
33
34
35
36
37

38 Introduction

39
40
41 As it has been largely demonstrated in literature, the epitaxy of oxide thin films on single
42
43 crystalline substrates usually requires high temperature during the growth ¹⁻⁵. However, for a lot
44
45 of industrial applications based on such epitaxial films, it would be necessary to reduce the growth
46
47 temperature to avoid atomic interdiffusion between film and substrate, and consequently to
48
49 significantly reduce the fabrication cost ⁶. In this framework, research activities have been carried
50
51 out to study room temperature (RT) epitaxial growth of oxide films like NiO ^{7,8}, Fe₃O₄ ⁹, V₂O₃ ¹⁰,
52
53 CoO and Co₃O₄ ¹¹, and other oxides ¹²⁻¹⁴. In most of these works, the RT epitaxial oxide films
54
55
56
57
58
59
60

1
2
3 were grown on atomically stepped single crystal sapphire (001) substrates by using the pulsed-laser
4 deposition (PLD) method ⁷⁻¹⁴. Such stepped c-cut sapphire substrates are obtained by a thermal
5 annealing process at high T (1000°C) for a few hours in air ^{15,16}. The surface steps play the role of
6 nucleation centers for the epitaxial growth of the film. On the other hand, PLD is used for the film
7 growth at RT owing to one of the specificities of this method, i.e. the high kinetic energy of the
8 species emitted by the target during laser irradiation. Indeed, such a high kinetic energy (about a
9 few 10th eV) ¹⁷ allows a high surface mobility for the species that leads to the formation of
10 crystalline material at relatively low temperature ^{18,19}.

21
22 In addition to the RT epitaxial growth of oxide films on c-cut (001 oriented) sapphire
23 substrates, some other papers report the RT epitaxy of oxide films on single crystal substrates like
24 MgO ²⁰, SrTiO₃ ²¹, bare Si ²²⁻²⁴ or Si covered by a buffer layer ²⁵. However, some other single
25 crystal substrates like a-cut ((110) oriented) and r-cut ((102) oriented) sapphire substrates are
26 currently used for the epitaxial growth of various oxide films ²⁶⁻³¹ with a view of specific
27 applications ³²⁻³⁴. To our knowledge, the RT epitaxy of oxide films on such a-cut and r-cut sapphire
28 substrates has never been reported.

29
30 In this frame, we have studied the growth by PLD at RT of Zn-doped iron oxide on a-cut
31 and r-cut sapphire substrates. For comparison purpose, ZFO films were also grown on a c-cut
32 substrate, but more complex results obtained with this substrate will be published later in a
33 forthcoming paper. Owing to the experimental PLD conditions used, two iron oxide-based phases
34 are obtained: the Zn-doped wüstite phase Zn:FeO that will be noted "ZFO_w" in the following and
35 the Zn-doped Zn:Fe₃O₄ spinel magnetite phase (noted "ZFO_s"). More precisely, Zn_{1-x}Fe_xO films
36 with (0 < x < 1) can be grown by PLD: following previous work³⁵, the Zn:Fe₃O₄ phase is obtained
37 for 0.65 < x < 1. We have chosen a Zn concentration fixed at around 25% at. (x = 0.75) to avoid the
38
39
40
41
42
43
44
45
46
47
48
49
50
51
52
53
54
55
56
57
58
59
60

1
2
3 formation of the wurtzite phase. In addition, the presence of Zn in the iron oxide phases should
4 promote the growth the wüstite phase even at low temperature ($T < 500^{\circ}\text{C}$) as evidenced by Sano
5 et al.³⁶. We present here a detailed structural study of these phases deposited at RT on the various
6 sapphire substrates: growth, textures and epitaxial relationships between these compounds and the
7 different substrates are discussed. Such films could be of interest due to their magnetic properties
8 since wüstite-based films are expected to be antiferromagnetic while magnetite-based films should
9 be ferrimagnetic. These properties would permit the development of magnetite-based storage or
10 spintronics devices^{37,38}, while wüstite could be used as a transparent p-type conductors³⁹ or for
11 magneto-resistance enhancement⁴⁰. However, these interesting physical properties are not the
12 subject of this paper which is devoted to the detailed study of the structural properties of these
13 films.
14
15
16
17
18
19
20
21
22
23
24
25
26
27
28
29

30 In our work, in contrary to the common high T annealing of the substrates before the film
31 growth, all the c-, a- and r-cut sapphire substrates were not submitted to a thermal treatment at
32 high T before the growth. Despite this point, we obtained the epitaxial growth at RT of the Zn-
33 doped wüstite (ZFO_w , space group $Fm-3m$) and/or spinel (ZFO_s , $Fd-3m$) phases in the films.
34 Different textures were obtained for these phases on the following type of substrates, i.e. (111) for
35 the c-cut and a-cut sapphire, and (001) for the r-cut one. Well-defined epitaxial relationships were
36 found between films and substrates, and they have been described in the frame of the “domain
37 matching epitaxy” (DME)⁴¹⁻⁴⁴. The different textures observed depending on the substrates, could
38 be explained either by (i) the graphoepitaxy related to the presence of steps and terraces on the c-
39 cut and a-cut substrates⁴⁴⁻⁴⁶, (ii) a “quasi van der Waals epitaxy” related to the polar nature of the
40 c-cut and a-cut substrate plane and/or film plane⁴⁷⁻⁵⁰, and (iii) an epitaxy related to a low lattice
41 mismatch between the film and substrate in the case of the r-cut sapphire substrate.
42
43
44
45
46
47
48
49
50
51
52
53
54
55
56
57
58
59
60

Experimental section

The Zn-doped iron oxide films were grown by PLD onto c-cut, a-cut and r-cut sapphire substrates at RT in vacuum. The substrates furnished by CrysTec GmbH were not annealed at high T before the growth. A frequency quadrupled Nd-doped yttrium aluminum garnet (Nd:YAG) laser (266 nm, $\tau = 7$ ns) was used to ablate a Zn:Fe₃O₄ (Zn_{0.85}Fe_{2.15}O₄) target in the experimental set up already described elsewhere⁵¹. The PLD growth from a Zn:Fe₃O₄ target can lead to the formation of nanocomposite films^{52,53}, i.e. with the presence of the wüstite (Zn:FeO) and spinel (Zn:Fe₃O₄). In contrary to the spinel phase, which has been epitaxially grown at RT⁹, the wüstite phase has never been obtained in these conditions. In our work, we have tried to favor the growth conditions for the epitaxy of the wüstite phase at RT. Indeed, the difference in oxygen composition between the wüstite, [O]/[Fe] = 1.1, and the spinel, [O]/[Fe] = 1.33, means that the film must be grown under a low oxygen pressure. PLD allows oxygen incorporation in the oxide films to be controlled⁵⁴⁻⁵⁸. On one hand, the films on a-cut and r-cut substrates were thus grown under reducing conditions (residual vacuum: $2 \cdot 10^{-7}$ mbar), i.e. a priori the ideal conditions for the formation of the wüstite phase. On the other hand, the ZFO film on c-cut substrate was grown at $7 \cdot 10^{-6}$ mbar leading to the presence of both wüstite and spinel phase.

Atomic force microscopy (AFM) was used to study the surface topography of the bare substrates before the growth, using an AFM NT-MDT Ntegra instrument.

Rutherford backscattering spectrometry (RBS) using the 2.5 MeV ion accelerator (SAFIR) of the Sorbonne Université, allowed the film thickness and in-depth distribution of the elements to be determined. The spectra, not presented here, show that the Zn-doped iron oxide films are only constituted by Fe, Zn and O atoms, without the presence of any impurities. The precise

1
2
3 concentration profile of the Zn, Fe and O elements has been obtained from the simulation of the
4
5 RBS spectra by use of the RUMP simulation program and has allowed to deduce the [O]/[Fe] ratio
6
7 in the films.
8
9

10
11 X-ray diffraction (XRD) has been performed on a Bruker D8 Advance θ - 2θ diffractometer
12
13 in modified Bragg-Brentano geometry, working with monochromatized Cu $K\alpha_1$ radiation ($\lambda =$
14
15 1.5406 Å) and equipped with a LynxEye detector. The sample was rotated at a speed of 30 rpm
16
17 during measurement. Le Bail profile refinement using the Fullprof software⁵⁹ of the XRD patterns
18
19 of ZFO films grown on a-cut and r-cut sapphires enabled to precise unambiguously whether ZFO_w
20
21 and ZFO_s phases are both present and to estimate the cell parameters of these phases. For these
22
23 refinements, the “zero”-shifts due to the sample positioning were first determined from the 2θ -
24
25 shifts of the substrate Bragg peaks, and then fixed to enable the refinement of the cell parameters
26
27 of the iron oxide phases. The texture of the films and the in-plane relationships with the substrate
28
29 were investigated by pole figure measurements with the help of a Bruker D8 Discover
30
31 diffractometer (Cu $K\alpha_{1,2}$ radiation).
32
33
34
35
36
37

38 For transmission electron microscopy (TEM) observations, thin foils were thinned down
39
40 to electron transparency by a focused ion beam (FIB) setup (Dual-beam FEI Helios nanolab 660)
41
42 with an electron imaging resolution of 0.6 nm at 15 kV (Field emission gun (FEG)) and a FIB
43
44 resolution of 2.54 nm at 30 kV. TEM experiments were performed using a double corrected cold
45
46 FEG JEOL ARM 200F microscope, operated at 200 kV and equipped with a post column GATAN
47
48 QUANTUM ER electron energy loss spectrometer (EELS). This microscope had also a scanning
49
50 setup (STEM mode with dark and bright field detectors) allowing the electron beam to be
51
52 monitored with a spatial resolution of about 0.078 nm. Altogether, STEM EELS experiments were
53
54
55
56
57
58
59
60

1
2
3 then possible in order to obtain EELS spectra for a nanometer region, EELS profiles or even EELS
4 mapping. All digitized images and spectral data were processed using the commercial
5 Digitalmicrograph (GMS2) software from GATAN.
6
7
8
9
10
11
12
13

14 Results

15
16
17 Before the RT growth of ZFO films on the single crystal substrates, AFM images of the
18 surface of these substrates were registered. Figure 1 shows the surface morphology of the c-cut
19 (Fig. 1(a)), a-cut (Fig. 1(b)) and r-cut (Fig. 1(c)) sapphire substrates as furnished by CrysTec
20 GmbH.
21
22
23
24
25
26
27

28 Both c-cut and a-cut sapphire substrates show not very well defined and very narrow steps
29 without terraces, while the surface of the r-cut sapphire does not show any steps or terraces but
30 only a few spikes. This work mainly aimed at checking the possible RT epitaxy of ZFO films on
31 a- and r-cut sapphire substrates. First, we have looked at the possible RT epitaxy of ZFO on a c-
32 cut substrate. Indeed, the RT epitaxy of Zn (25%at.) doped Fe₃O₄ has not been previously reported
33 on c-cut substrate. Therefore, the PLD growth of such a film on a c-cut substrate at RT under a
34 7x10⁻⁶ mbar oxygen pressure has been studied. Figure 2 reports the corresponding XRD pattern of
35 such film and shows first, a broad peak at about 18° related to the (111) spinel phase with refined
36 cell parameter $a_s = 0.8529 \pm 0.0005$ nm, i.e. higher than the expected theoretical value for undoped
37 Fe₃O₄ ($a = 0.83905$ nm, $Fd-3m$). Secondly, a broad asymmetric peak around 36° corresponding to
38 the superimposition of 222 spinel and the 111 wüstite Bragg reflections is observed. Despite the
39 low intensity of the 111 ZFO_w peak, the cell parameter is around $a_w = 0.43217 \pm 0.0005$ nm, a
40 value slightly higher than for the undoped FeO phase ($a = 0.4307$ nm, $Fm-3m$) (Table 1).
41
42
43
44
45
46
47
48
49
50
51
52
53
54
55
56
57
58
59
60

Table 1. Composition determined by RBS and crystallographic features determined by XRD of ZFO films grown at RT on c-cut, a-cut and r-cut sapphires (W: wüstite, S: spinel). The values of [O]/[Fe] does not consider oxygen bound to zinc and are only related to oxygen associated to iron.

Substrate	Composition	[O]/[Fe]	a_w	a_s	Preferential orientation	FWHM RC
c-cut	$Zn_{0.24}Fe_{0.76}O_{1.15}$ ($Zn_{0.24}O_{0.24}$)($Fe_{0.76}O_{0.91}$)	1.19	0.43217 ± 0.005 nm	0.85289 ± 0.005 nm	(111) W (111) S	$\sim 1.8^\circ$
a-cut	$Zn_{0.23}Fe_{0.77}O_{1.12}$ ($Zn_{0.23}O_{0.23}$)($Fe_{0.77}O_{0.89}$)	1.15	0.43435 ± 0.005 nm	-	(111) W	$\sim 1.9^\circ$
r-cut	$Zn_{0.23}Fe_{0.77}O_{1.1}$ ($Zn_{0.23}O_{0.23}$)($Fe_{0.77}O_{0.87}$)	1.13	0.4317 ± 0.005 nm	0.8415 ± 0.005 nm	(100) W (100) S	4.7°

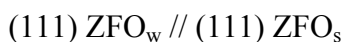
TEM analysis was led to precisely investigate the epitaxial growth of the ZFO film on c-cut sapphire substrate. Figure 3(a) shows a typical high resolution electron microscopy (HREM) image of a cross section of the film. The orientation of the sample is such that the electron beam is parallel to the [210] direction of Al_2O_3 sapphire (visible at the bottom of the image) and thus parallel to the film/substrate interface. In the upper region of the film, one can notice distinctly that we are dealing with a columnar growth with column widths of a few tens of nanometers whereas the bottom of the film appears more “uniform” without visible boundaries over a thickness of about 15 nm by contrast with the upper region.

By extracting and enlarging smaller regions from these parts of the film (shown in Fig. 3(b) for the rough images and 3(c) for the corresponding filtered images), an analysis of the lattice

1
2
3 fringes through Fast Fourier Transforms (FFTs) allows establishing the structural characteristics
4 and then the corresponding phases. The FFTs presented in Fig. 3(d) reveal that the bottom part of
5 the film is consistent with a face centered cubic structure along a [-101] direction with a lattice
6 parameter of 0.43 nm. This agrees with the wüstite phase (FeO) doped with Zn (confirmed by
7 chemical analyses, not shown). The corresponding orientation relationships between sapphire and
8 ZFO_w are the following:
9



10
11
12
13
14
15
16
17
18
19
20
21
22
23
24
25 As far as the upper region is concerned, the FFT of the enlarged image shows also a face
26 centered cubic structure but with a lattice parameter close to that of the spinel phase Fe₃O₄. Zn is
27 also present in the chemical composition of the compound and the orientation relationships
28 between wüstite and magnetite are:
29
30
31
32



33
34
35
36
37
38
39
40
41 To confirm the presence of both phases, a spectroscopic analysis using EELS method has
42 been used. In Fig. 3(a), two spots are indicating the two pointed regions from which one obtained
43 the EELS spectra presented in Fig. 4.
44
45
46
47
48

49 These spectra correspond to the L₂ and L₃ thresholds of Fe whose positions are indicative
50 of the valence state of Fe. A 1 eV displacement of the L₃ peak towards lower energies for the bottom
51 of the film is clearly meaning a decrease in the valence state of Fe and then consistent with the
52
53
54
55
56
57
58
59
60

1
2
3 presence of the wüstite phase at the bottom of the film. Similar shift for these compounds has been
4 reported in previous works ⁶⁰. The presence of the wüstite phase is also in agreement with the
5 [O]/[Fe] ratio deduced from RBS measurements, the obtained values being between 1.13 and 1.19
6
7 (Table 1).
8
9
10
11
12

13 The XRD θ - 2θ patterns recorded on the ZFO films grown on the a- and r-cut substrates are
14 presented in Fig. 5. The data regarding the lattice parameters and the full width at half maximum
15 (FWHM) of the rocking curves are summarized in Table 1. The XRD pattern (Fig. 5(a)) recorded
16 for the film grown on the a-cut sapphire shows the presence of the 111 wüstite reflection at about
17 $2\theta = 35.75^\circ$. The 111 and 222 spinel peaks which would appear at 18° and 36.6° respectively, are
18 not observed in this pattern. Profile refinement using a single FeO phase leads to satisfying
19 modelisation of the observed peak and suggests that the film is constituted of a pure wüstite phase.
20
21
22
23
24
25
26
27
28
29

30 In Fig. 5(b), the XRD pattern corresponding to the film grown on the r-cut substrate shows
31 a wide peak at about 41.75° . Best profile refinement is obtained by considering simultaneous
32 presence of 200 and 400 Bragg reflections of ZFO_w and ZFO_s phases, respectively, showing a
33 significant texture of these films. Due to the limited number of observed diffraction peaks, it is not
34 possible to retrieve the proportional distribution of each phase from the refinement.
35
36
37
38
39
40
41
42

43 For the ZFO films grown on the a-cut substrate, the rocking curve (not shown here) of the
44 respective 111 reflection peaks is rather narrow, i.e. 1.9° , taking into account the RT growth. On
45 the contrary, for the ZFO film grown on the r-cut substrate, the value of the rocking curve of the
46 002 ZFO_w reflection was much more important, i.e. 4.7° . In this latter case, the crystalline quality
47 of the film is poorer. It must be noticed that in the case of the epitaxial growth of various oxide
48 films on r-cut sapphire substrate, the surface plane of the oxide film was tilted with respect to the
49
50
51
52
53
54
55
56
57
58
59
60

(102) plane of sapphire. This phenomenon was observed for instance in the epitaxial growth of ZnO⁶¹, CeO₂⁶², MgO^{63,64} or Fe₃O₄⁶⁵. The tilt can be important, for example the (100) MgO may epitaxially grow on (102) Al₂O₃ with a tilt up to 5 or 6°, depending upon the growth temperature. From such results, it was concluded that the surface state of r-plane sapphire is an important factor leading to the tilted growth of the epilayer⁶³⁻⁶⁵. In our present case, it is not surprising that the epitaxial growth of ZFO on r-plane Al₂O₃ occurs at RT with a tilt of about 4.7°.

Figure 6(a) shows the results of the epitaxial relationships study between the wüstite phase and the a-cut substrate. The phi-scan performed on the {200} planes of the ZFO_w phase ($2\theta = 42.391^\circ$; $\psi = 56.22^\circ$) shows 6 peaks separated by 60°. In addition, phi-scan of the {104} planes of sapphire ($2\theta = 35.14^\circ$; $\psi = 57.55^\circ$) was also performed to deduce the crystalline orientations of the film with respect to the substrate. It shows 2 peaks separated by 180° and located at about 6.2° of the closest peak of the film. Figure 6(b) shows the pole figure recorded with the 200 ZFO_w reflection ($2\theta = 42.39^\circ$) for the same film grown on the a-cut substrate. This figure presents 6 well defined poles at ψ equal to 56.22°, in agreement with the phi-scan in Fig. 6(a). Some other poles from the substrate are also observed at: i) $\psi = 29^\circ$ corresponding to the 113 Al₂O₃ reflection (owing to the angle between (110) and (113) planes (28.78°) and the Bragg reflection of (113) plane: $2\theta = 43.36^\circ$) and ii) $\psi = 64^\circ$ corresponding to the -123 Al₂O₃ reflection (angle between (110) and (113) planes = 64.01° and $2\theta (-123) = 43.36^\circ$).

From the azimuthal positions of the respective peak/poles of ZFO_w and Al₂O₃, it is demonstrated that the epitaxial relationships on the a-cut sapphire substrate correspond to the superposition of the hexagons of the (111) ZFO_w plane on the rectangular lattice of the a-cut

sapphire, with a slight disorientation between the two lattices, as shown in Fig. 7(a). Given this pattern, no match can be observed between the two lattices.

Actually, the explanation of the epitaxial growth of ZFO_w on Al₂O₃ is in the frame of the domain matching epitaxy (DME), with m lattice units of the film matching with p lattice units of the substrate⁶⁴, as shown in figure 7(b). This figure presents the in-plane lattices of ZFO_w and sapphire which are superimposed considering the 6.2° of rotation between the (2-20) plane of ZFO_w and the (1-1-4) plane of the sapphire. The interception of these planes with the in-plane lattices (traces) corresponds to the traces of the (200) plane of ZFO_w and the (10-4) plane of the sapphire chosen to carry out the phi-scans measurement. It can be seen in figure 7(b) that there is a coincidence of sites between the two lattices leading to a matching domain forming a parallelogram. Since the Bravais lattice of the sapphire is hexagonal, it is not possible to easily determine the directions which correspond to the sides of this parallelogram. We have therefore described the epitaxial relationships between the two lattices by instead considering rather the planes which form the parallelogram, as follows:

Out-of-plane: (111) ZFO_w // (110) Al₂O₃

In-plane (I) (11-2) ZFO_w // (1-12) Al₂O₃

In-plane (II) (-871) ZFO_w // (1-1-4) Al₂O₃

In-plane (III) (3-1-2) ZFO_w // (1-1-1) Al₂O₃

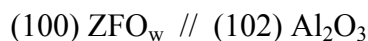
Only the shortest side of the parallelogram corresponds to a perfect fit of m lattice units ($m = 5$ for ZFO_w and $p = 1$ for Al₂O₃). Therefore, lattice mismatches are determined by considering

the interatomic distances shown in figure 7(c). It appears that these distances are very close between the two lattices, corresponding to low mismatch values (cf. Table 2).

Table 2. Epitaxial relationships of Zn:FeO wüstite films grown at RT on a-cut and r-cut sapphires.

Substrate	Epitaxial relationships	Domain matching relationships		Lattice mismatch δ (%)	Domain size D (nm)
		m	p		
a-cut	(11-2) ZFO _w // (1-12) Al ₂ O ₃	5	1	1.2	1.52
	(-871) ZFO _w // (1-1-4) Al ₂ O ₃	-	-	-1.38	2.12
	(3-1-2) ZFO _w // (1-1-1) Al ₂ O ₃	-	-	-2.21	2.78
r-cut	[100] ZFO _w // [010] Al ₂ O ₃	11	10	-0.06	4.7
	[010] ZFO _w // [2-1-1] Al ₂ O ₃	6	5	-1.28	2.6

Figure 8(a) displays the phi-scans of the ZFO film grown on r-cut sapphire recorded by selecting the {111} planes. It shows 4 peaks separated by 90° and located for the closest one at about 45.5° of the (006) substrate plane. The corresponding pole figure is shown in Fig. 8(b). Similarly, the pole figure (Fig. 8(b)) for the ZFO film grown on the r-plane Al₂O₃ was also recorded. From the azimuthal positions of the peaks/poles, the following epitaxial relationships were deduced:



1
2
3 Such orientation relationships correspond to the superposition of the square lattice plane
4 (001) of ZFO_w on the rectangular lattice of the (102) plane of Al_2O_3 substrate as shown in Fig.
5
6
7
8 9(a).
9

10
11 These two relationships lead in both case to rather large lattice mismatch, 9% for (I) and
12
13 15.6% for (II), respectively. Regarding the DME, as indicated in Table 2, a coincidence for relation
14
15 (I) is obtained with 10 substrate units and 11 film units giving a -0.06% lattice mismatch. For the
16
17 relation (II) the coincidence is realized with 5 substrate units and 6 film units with a -1.28%
18
19 mismatch (Fig. 9(b)).
20
21
22

23 Discussion

24
25
26
27 In the previous works reported on the RT epitaxy of oxide films, results were usually
28
29 obtained on c-cut sapphire substrates, and two main points play a role on this epitaxy. The first is
30
31 the presence of steps and terraces on the c-cut surface. These steps and terraces are due to a miscut
32
33 and / or a high T annealing of the c-cut sapphire substrate^{15,16}, which will play the role of
34
35 nucleation centers for the epitaxial growth. This kind of growth corresponds to the graphoepitaxy
36
37⁴⁶. The second point is the fact that the c-cut sapphire plane is polar, i.e. either a pure oxygen plane
38
39 or a pure Al plane. In the case of the cubic oxides (NiO , Co_3O_4 , Fe_3O_4 , ...), epitaxially grown at
40
41 RT or at high T on c-cut substrate, the observed texture is (111), i.e. a plane which is also a polar
42
43 plane⁴⁵. The epitaxial growth concerns thus two polar planes, and this situation is very similar to
44
45 the quasi van der Waals epitaxy^{48,49} where there is only very little or no chemical bonding between
46
47 the atoms of the film and substrate. Indeed, the stability and the epitaxy of the film-substrate
48
49 interface are related to the weak electrostatic interaction between the two polar planes⁵⁰.
50
51
52
53
54
55
56
57
58
59
60

1
2
3 In the case of the ZFO epitaxial growth on c-cut substrate, the epitaxial relationships are
4 the same as those observed in the case of the growth of ZFO on this substrate at elevated
5 temperature⁵², i.e. the growth occurs with a "30° rotation" of the hexagons of the (111) ZFO plane
6 on the hexagon of the (002) sapphire plane. It should be reminded that, in this work, the substrate
7 was not thermally treated, so the AFM image shows presence of steps, but however much less
8 defined than the ones obtained with a high thermal treatment at 1000°C. Moreover, after the film
9 growth, the AFM images (not shown) does not show any steps or terraces which is rather different
10 from the results commonly reported in which steps and terraces are present at the surface of the
11 oxide films grown at RT on c-cut substrates annealed at high temperature before the growth. In
12 our case, polar nature of the c-cut sapphire substrate and of the (111) plane of the Zn-doped iron
13 oxide may lead to an electrostatic interaction at this interface. Therefore, it seems reasonable to
14 conclude that both the graphoepitaxy and the quasi van der Waals epitaxy are at the origin of the
15 RT epitaxy of ZFO on c-cut sapphire substrate. Concerning the film grown on the a-cut substrate,
16 it must be noticed that this substrate is also either a pure cationic or a pure oxygen one. Our results
17 show that the RT epitaxy of the wüstite phase is based on the (111) ZFO_w plane, despite the fact
18 that the a-cut substrate and the (111) ZFO_w present very different atomic configuration, i.e. a
19 symmetry mismatch between the substrate (2-fold) and the (111) ZFO_w film (3-fold).
20
21
22
23
24
25
26
27
28
29
30
31
32
33
34
35
36
37
38
39
40
41
42

43 An interesting point which can be noticed is that such epitaxial relationship (111) ZFO_w //
44 (110) Al₂O₃ corresponds to an epitaxy of a hexagon on a rectangle with different symmetries for
45 these two planes. One can ask thus why an epitaxy with a square (ZFO_w) on a rectangle (r-cut
46 Al₂O₃) is not observed while the square and rectangular configurations would be more relevant.
47 Concerning the DME, it is possible to obtain the lattice mismatch δ and domain matching epitaxy
48
49
50
51
52
53
54
55
56
57
58
59
60

D in terms of the epitaxial relationships with (001) ZFO_w // (110) Al₂O₃. The calculated values of δ and D are the following:

$$[100] \text{ ZFO}_w // [001] \text{ Al}_2\text{O}_3 \quad m = 3 \quad p = 1 \quad \delta = 0.02 \% \quad D = 1.3 \text{ nm}$$

$$[001] \text{ ZFO}_w // [1-10] \text{ Al}_2\text{O}_3 \quad m = 19 \quad p = 10 \quad \delta = 0.13 \% \quad D = 8.3 \text{ nm}$$

The comparison of these values with those given in Table 2 for the (111) ZFO_w // (110) Al₂O₃ indicates that the epitaxy of the square (001) ZFO_w on the rectangular (110) Al₂O₃ is better in terms of DME. The reason why this epitaxy is not observed is certainly related to the fact that the (100) ZFO_w plane is not a polar plane, i.e. O and Fe are present in this plane. It can be concluded that the van der Waals epitaxy based on the electrostatic interaction between the (111) ZFO_w and the (110) Al₂O₃ is preferred to the simple “square on rectangular” epitaxy.

It follows thus that the (111) ZFO_w texture could be explained in the frame of an electrostatic interaction due to the “quasi Van der Waals epitaxy”. Indeed, the (111) plane in the wüstite (FCC structure) is a polar plane, and the a-cut sapphire plane is also a polar plane. An electrostatic interaction between these two polar planes is thus envisaged in a similar way to the quasi van der Waals epitaxy.

For the ZFO film grown on the r-cut substrate, the (100) wüstite texture is observed. This is rather surprising since this situation is *a priori* similar to the a-cut substrate case. Indeed, the r-cut plane is either a pure oxygen plane or a pure cationic plane, and it presents a rectangular atomic configuration. As for the a-cut surface plane, the (111) wüstite texture could be expected, but the (100) wüstite texture is observed. This means that both the graphoepitaxy and/or van der Waals epitaxy cannot be envisaged to explain the epitaxial growth of ZFO on the r-cut sapphire substrate.

1
2
3 We mentioned above the specific problem of the tilt in the epitaxy on r-cut substrate, but
4
5 another parameter is the growth temperature, which plays an important role in the epitaxial growth
6
7 of oxide films on the r-cut substrate. For example in the case of CeO₂ films grown on a r-cut
8
9 substrate thermally treated at high T (1000°C), steps and terraces are formed at the surface and a
10
11 pure (100) CeO₂ texture is observed for example ^{28,67,68}. Moreover, the steps are formed along the
12
13 [010] direction of the r-cut substrate, which is one of the in-plane directions of the epitaxy. On the
14
15 contrary, when the r-cut substrate is not thermally treated at high temperature, steps and terraces
16
17 are not formed, and both (111) and (100) CeO₂ textures are observed ^{28,67,68}. Further studies on
18
19 CeO₂ films on r-cut substrates have shown that the growth temperature plays an important role on
20
21 the film texture ⁶⁹. Indeed, the texture of CeO₂ films changed from (001) at 150°C to a mixed (001)
22
23 and (111) textures at 300°C, and finally to pure (111) for increasing temperatures ⁴. In our work,
24
25 the presence of steps and terraces on the r-cut substrate (Fig. 1(c)) is not clearly evidenced from
26
27 the AFM images, and furthermore only the (100) ZFO_w texture is observed. Moreover, our films
28
29 are grown at RT, and we can thus assume that the (100) ZFO_w texture is due to the low growth
30
31 temperature of the film in a similar way to the case of the CeO₂ film grown on r-cut sapphire
32
33 substrates ⁶⁹.
34
35
36
37
38
39
40

41 **Conclusion**

42
43
44 Using a Zn:FeO_x target, the wüstite (Zn:FeO) and/or spinel (Zn:Fe₃O₄) phases were
45
46 obtained on c-cut, a-cut and r-cut sapphire single crystal substrates by pulsed laser deposition at
47
48 room temperature. Depending upon substrates, the two textures, (111) or (100), may be obtained,
49
50 and poles figures showed the RT epitaxy of the films on all substrates. The possible origin of these
51
52 distinct textures and epitaxial relationships has been discussed according to both the
53
54 « graphoepitaxy » and the « quasi van der Waals epitaxy » for the films grown on the c-cut and a-
55
56
57
58
59
60

1
2
3 cut substrates. For the film grown on the r-cut, the (100) texture is obtained as it has been observed
4
5 in other cases. An important point in the RT epitaxy of the ZFO films is the high kinetic energy of
6
7 the species emitted by the target during the laser ablation. Such a high kinetic energy of these
8
9 species will give them the possibility to move on the substrate on sufficient long distances to find
10
11 their site in the growth of the crystal structure. Finally, this work shows that the RT epitaxy of the
12
13 oxide films is quite possible on various sapphire substrates (c-cut, a-cut and r-cut), and this opens
14
15 the way to the PLD growth of oxide films on substrates like MgO, MgAl₂O₄ or others at RT.
16
17
18
19
20
21
22
23
24
25
26

27 AUTHOR INFORMATION

31 Corresponding Author

32
33
34
35 *Information for the author to whom correspondence should be addressed: Dr. Valerie Demange.

36
37
38 Valerie.demange@univ-rennes.fr
39
40
41

42 Author Contributions

43
44
45 The manuscript was written through contributions of all authors. All authors have given approval
46
47 to the final version of the manuscript. VD performed the XRD characterizations and LeBail
48
49 refinement, analyzed and interpreted the corresponding data and drafted the article. XP performed
50
51 the TEM and EELS measurements, analyzed and interpreted the corresponding data and drafted
52
53 the article. SO performed the AFM measurements. MP and TR performed LeBail refinement,
54
55
56
57
58
59
60

1
2
3 analyzed and interpreted the corresponding data. CH and MN synthesized PLD films, performed
4
5 RBS measurements, analyzed and interpreted the corresponding data. MGV revised the
6
7 manuscript. CC and EM analyzed and interpreted the data and drafted the article. JP conceived
8
9 and designed the project, analyzed and interpreted the data and drafted the article.
10
11
12

13 **Funding Sources**

14
15
16
17 The research of the manuscript was supported by the French ANR (Agence Nationale de la
18
19 Recherche) organisation and the Normandie Region in acquiring the EELS spectrometer and the
20
21 FIB setup in the framework of the PAI program (ANR-11-EQPX-0020). XRD measurements were
22
23 performed on Osirix platform (ScanMAT, UAR 2025 University of Rennes-CNRS), which
24
25 received a financial support from the European Union through the European Regional
26
27 Development Fund (ERDF), the Département d'Ille et Vilaine, Rennes Métropole and Région
28
29 Bretagne (2015-2020 CPER project SCANMAT).
30
31
32

33 **ACKNOWLEDGMENT**

34
35
36
37 XP thanks Franck LEMARIE for his contribution in preparing the TEM samples. The agreement
38
39 on cooperation between the National Institute for Lasers, Plasma and Radiation Physics (NILPRP)
40
41 and the INSP, Université Pierre et Marie Curie –Paris 6 (now Sorbonne Université) is also
42
43 acknowledged (M.N., J.P.).
44
45
46

47 **ABBREVIATIONS**

48
49 RT, room temperature; PLD, pulsed-laser deposition; ZFO_w, wüstite phase Zn:FeO; ZFO_s, Zn-
50
51 doped Zn:Fe₃O₄ spinel magnetite phase; Nd:YAG, Nd-doped yttrium aluminum garnet; AFM,
52
53 atomic force microscopy; RBS, Rutherford backscattering spectrometry; XRD, X-ray diffraction;
54
55
56
57
58
59
60

1
2
3 TEM, transmission electron microscopy; FIB, focused ion beam; FEG, Field emission gun; EELS,
4 electron energy loss spectrometer; STEM, scanning transmission electron microscopy; HREM,
5 high resolution electron microscopy; FFT, Fast Fourier Transform; FWHM, full width at half
6 maximum; DME, domain matching epitaxy.
7
8
9
10
11
12

13 REFERENCES

- 14
15
16
17 (1) Chambers, S. A. Epitaxial Growth and Properties of Doped Transition Metal and Complex
18 Oxide Films. *Adv. Mater.* **2010**, *22* (2), 219–248. <https://doi.org/10.1002/adma.200901867>.
19
20
21 (2) Narayan, J. Recent Progress in Thin Film Epitaxy across the Misfit Scale (2011 Acta Gold
22 Medal Paper). *Acta Mater.* **2013**, *61* (8), 2703–2724.
23
24 <https://doi.org/10.1016/j.actamat.2012.09.070>.
25
26
27 (3) Roemer, A.; Millon, E.; Vincent, B.; Boudrioua, A.; Pons-Y-Moll, O.; Defourneau, R. M.;
28 Seiler, W. Epitaxial PbTiO₃ Thin Films Grown on (100) MgO by Pulsed-Laser Deposition for
29 Optical Waveguiding Properties. *J. Appl. Phys.* **2004**, *95* (6), 3041–3047.
30
31 <https://doi.org/10.1063/1.1649461>.
32
33
34 (4) Nistor, M.; Seiler, W.; Hebert, C.; Matei, E.; Perrière, J. Effects of Substrate and Ambient
35 Gas on Epitaxial Growth Indium Oxide Thin Films. *Appl. Surf. Sci.* **2014**, *307*, 455–460.
36
37 <https://doi.org/10.1016/j.apsusc.2014.04.056>.
38
39
40 (5) Tricot, S.; Nistor, M.; Millon, E.; Boulmer-Leborgne, C.; Mandache, N. B.; Perrière, J.;
41 Seiler, W. Epitaxial ZnO Thin Films Grown by Pulsed Electron Beam Deposition. *Surf. Sci.* **2010**,
42 *604* (21), 2024–2030. <https://doi.org/10.1016/j.susc.2010.08.016>.
43
44
45 (6) Rasic, D.; Sachan, R.; Chisholm, M. F.; Prater, J.; Narayan, J. Room Temperature Growth
46 of Epitaxial Titanium Nitride Films by Pulsed Laser Deposition. *Cryst. Growth Des.* **2017**, *17* (12),
47 6634–6640. <https://doi.org/10.1021/acs.cgd.7b01278>.
48
49
50
51
52
53
54
55
56
57
58
59
60

- 1
2
3 (7) Yamauchi, R.; Hamasaki, Y.; Shibuya, T.; Saito, A.; Tsuchimine, N.; Koyama, K.;
4 Matsuda, A.; Yoshimoto, M. Layer Matching Epitaxy of NiO Thin Films on Atomically Stepped
5 Sapphire (0001) Substrates. *Sci. Rep.* **2015**, *5* (1), 14385. <https://doi.org/10.1038/srep14385>.
6
7
8
9
10 (8) Kakehi, Y.; Nakao, S.; Satoh, K.; Kusaka, T. Room-Temperature Epitaxial Growth of
11 NiO(111) Thin Films by Pulsed Laser Deposition. *J. Cryst. Growth* **2002**, *237–239*, 591–595.
12 [https://doi.org/10.1016/S0022-0248\(01\)01964-9](https://doi.org/10.1016/S0022-0248(01)01964-9).
13
14
15
16
17 (9) Liu, X.; Lu, H.; He, M.; Wang, L.; Shi, H.; Jin, K.; Wang, C.; Yang, G. Room-Temperature
18 Layer-by-Layer Epitaxial Growth and Characteristics of Fe₃O₄ Ultrathin Films. *J. Phys. Appl.*
19 *Phys.* **2014**, *47* (10), 105004. <https://doi.org/10.1088/0022-3727/47/10/105004>.
20
21
22
23
24 (10) Liu, X.; Lu, H.; He, M.; Jin, K.; Yang, G. Room-Temperature Epitaxial Growth of V₂O₃
25 Films. *Sci. China Phys. Mech. Astron.* **2014**, *57* (10), 1866–1869. [https://doi.org/10.1007/s11433-](https://doi.org/10.1007/s11433-014-5483-4)
26 [014-5483-4](https://doi.org/10.1007/s11433-014-5483-4).
27
28
29
30
31 (11) Matsuda, A.; Yamauchi, R.; Shiojiri, D.; Tan, G.; Kaneko, S.; Yoshimoto, M. Room-
32 Temperature Selective Epitaxial Growth of CoO (111) and Co₃O₄ (111) Thin Films with Atomic
33 Steps by Pulsed Laser Deposition. *Appl. Surf. Sci.* **2015**, *349*, 78–82.
34 <https://doi.org/10.1016/j.apsusc.2015.04.205>.
35
36
37
38
39
40 (12) Takakazu Kiyomura, T. K.; Manabu Gomi, M. G. Room-Temperature Epitaxial Growth of
41 Ni-Zn Ferrite Thin Films by Pulsed Laser Deposition in High Vacuum. *Jpn. J. Appl. Phys.* **1997**,
42 *36* (8A), L1000. <https://doi.org/10.1143/JJAP.36.L1000>.
43
44
45
46
47 (13) Yoshimoto, M.; Yamauchi, R.; Shiojiri, D.; Tan, G.; Kaneko, S.; Matsuda, A. Room-
48 Temperature Synthesis of Epitaxial Oxide Thin Films for Development of Unequilibrium Structure
49 and Novel Electronic Functionalization. *J. Ceram. Soc. Jpn.* **2013**, *121* (1409), 1–9.
50 <https://doi.org/10.2109/jcersj2.121.1>.
51
52
53
54
55
56
57
58
59
60

- 1
2
3 (14) Seo, O.; Tayal, A.; Kim, J.; Song, C.; Chen, Y.; Hiroi, S.; Katsuya, Y.; Ina, T.; Sakata, O.;
4
5 Ikeya, Y.; Takano, S.; Matsuda, A.; Yoshimoto, M. Tuning of Structural, Optical Band Gap, and
6
7 Electrical Properties of Room-Temperature-Grown Epitaxial Thin Films through the Fe₂O₃:NiO
8
9 Ratio. *Sci. Rep.* **2019**, *9* (1), 4304. <https://doi.org/10.1038/s41598-019-41049-9>.
- 10
11
12 (15) Yoshimoto, M.; Maeda, T.; Ohnishi, T.; Koinuma, H.; Ishiyama, O.; Shinohara, M.; Kubo,
13
14 M.; Miura, R.; Miyamoto, A. Atomic-Scale Formation of Ultrasoother Surfaces on Sapphire
15
16 Substrates for High-Quality Thin-Film Fabrication. *Appl. Phys. Lett.* **1995**, *67*, 2615.
- 17
18
19 (16) Yoshimoto, M.; Sasaki, A.; Akiba, S. Nanoscale Epitaxial Growth Control of Oxide Thin
20
21 Films by Laser Molecular Beam Epitaxy—towards Oxide Nanoelectronics. *Sci. Technol. Adv.*
22
23 *Mater.* **2004**, *5* (4), 527–532. <https://doi.org/10.1016/j.stam.2004.02.010>.
- 24
25
26 (17) Gudmundsson, J. T.; Anders, A.; Keudell, A. von. Foundations of Physical Vapor
27
28 Deposition with Plasma Assistance. *Plasma Sources Sci. Technol.* **2022**, *31* (8), 083001.
29
30 <https://doi.org/10.1088/1361-6595/ac7f53>.
- 31
32
33 (18) Craciun, V.; Singh, R. K.; Perriere, J.; Spear, J.; Craciun, D. Epitaxial ZnO Films Grown
34
35 on Sapphire (001) by Ultraviolet-Assisted Pulsed Laser Deposition. *J. Electrochem. Soc.* **2000**,
36
37 *147* (3), 1077. <https://doi.org/10.1149/1.1393316>.
- 38
39
40 (19) Nistor, M.; Millon, E.; Cachoncinlle, C.; Seiler, W.; Jedrecy, N.; Hebert, C.; Perrière, J.
41
42 Transparent Conductive Nd-Doped ZnO Thin Films. *J. Phys. Appl. Phys.* **2015**, *48* (19), 195103.
43
44 <https://doi.org/10.1088/0022-3727/48/19/195103>.
- 45
46
47 (20) Tachiki, M.; Hosomi, T.; Kobayashi, T. Room-Temperature Heteroepitaxial Growth of
48
49 NiO Thin Films Using Pulsed Laser Deposition. *Jpn. J. Appl. Phys.* **2000**, *39* (4R), 1817.
50
51 <https://doi.org/10.1143/JJAP.39.1817>.
- 52
53
54
55
56
57
58
59
60

- 1
2
3 (21) Ohnishi, T.; Yoshimoto, M.; Lee, G. H.; Maeda, T.; Koinuma, H. Unit Cell Layer-by-Layer
4 Heteroepitaxy of BaO Thin Films at Temperatures as Low as 20 °C. *J. Vac. Sci. Technol. A* **1997**,
5
6 *15* (5), 2469–2472. <https://doi.org/10.1116/1.580911>.
7
8
9
10 (22) Yoshimoto, M.; Shimozone, K.; Maeda, T.; Ohnishi, T.; Kumagai, M.; Chikyow, T.;
11
12 Ishiyama, O.; Shinohara, M.; Koinuma, H. K. H. Room-Temperature Epitaxial Growth of CeO₂
13
14 Thin Films on Si(111) Substrates for Fabrication of Sharp Oxide/Silicon Interface. *Jpn. J. Appl.*
15
16 *Phys.* **1995**, *34* (6A), L688. <https://doi.org/10.1143/JJAP.34.L688>.
17
18
19 (23) Furusawa, M.; Tashiro, J.; Sasaki, A.; Nakajima, K.; Takakura, M.; Chikyow, T.; Ahmet,
20
21 P.; Yoshimoto, M. In Situ Analysis of the Room-Temperature Epitaxial Growth of CeO₂ Ultrathin
22
23 Films on Si (111) by Coaxial Impact-Collision Ion Scattering Spectroscopy. *Appl. Phys. Lett.*
24
25 **2001**, *78* (13), 1838–1840. <https://doi.org/10.1063/1.1356451>.
26
27
28 (24) Ami, T.; Ishida, Y.; Nagasawa, N.; Machida, A.; Suzuki, M. Room-Temperature Epitaxial
29
30 Growth of CeO₂(001) Thin Films on Si(001) Substrates by Electron Beam Evaporation. *Appl.*
31
32 *Phys. Lett.* **2001**, *78* (10), 1361–1363. <https://doi.org/10.1063/1.1351849>.
33
34
35 (25) Tashiro, J.; Sasaki, A.; Akiba, S.; Satoh, S.; Watanabe, T.; Funakubo, H.; Yoshimoto, M.
36
37 Room-Temperature Epitaxial Growth of Indium Tin Oxide Thin Films on Si Substrates with an
38
39 Epitaxial CeO₂ Ultrathin Buffer. *Thin Solid Films* **2002**, *415* (1), 272–275.
40
41 [https://doi.org/10.1016/S0040-6090\(02\)00623-5](https://doi.org/10.1016/S0040-6090(02)00623-5).
42
43
44 (26) Zhu, Z.; Ma, J.; Luan, C.; Mi, W.; Lv, Y. Twin Structures of Epitaxial SnO₂ Films Grown
45
46 on A-Cut Sapphire by Metalorganic Chemical Vapor Deposition. *J. Vac. Sci. Technol. A* **2012**, *30*
47
48 (2), 021503. <https://doi.org/10.1116/1.3683042>.
49
50
51
52
53
54
55
56
57
58
59
60

- 1
2
3 (27) Kim, D. H.; Kwon, J.-H.; Kim, M.; Hong, S.-H. Structural Characteristics of Epitaxial
4 SnO₂ Films Deposited on A- and m-Cut Sapphire by ALD. *J. Cryst. Growth* **2011**, *322* (1), 33–
5
6 37. <https://doi.org/10.1016/j.jcrysgro.2011.03.004>.
7
8
9
10 (28) Kurian, J.; Naito, M. Growth of Epitaxial CeO₂ Thin Films on R-Cut Sapphire by
11 Molecular Beam Epitaxy. *Phys. C Supercond.* **2004**, *402* (1), 31–37.
12
13 <https://doi.org/10.1016/j.physc.2003.08.007>.
14
15
16
17 (29) Sunder, M.; Moran, P. D. How R-Plane Al₂O₃ Surface Modifications Impact the Growth
18 of Epitaxial (001) CeO₂ Thin Films. *J. Electron. Mater.* **2009**, *38* (9), 1931–1937.
19
20 <https://doi.org/10.1007/s11664-009-0864-6>.
21
22
23
24 (30) Pant, P.; Budai, J. D.; Aggarwal, R.; Narayan, R. J.; Narayan, J. Thin Film Epitaxy and
25 Structure Property Correlations for Non-Polar ZnO Films. *Acta Mater.* **2009**, *57* (15), 4426–4431.
26
27 <https://doi.org/10.1016/j.actamat.2009.05.031>.
28
29
30
31 (31) Han, S. K.; Hong, S. K.; Lee, J. W.; Lee, J. Y.; Song, J. H.; Nam, Y. S.; Chang, S. K.;
32 Minegishi, T.; Yao, T. Structural and Optical Properties of Non-Polar A-Plane ZnO Films Grown
33 on R-Plane Sapphire Substrates by Plasma-Assisted Molecular-Beam Epitaxy. *J. Cryst. Growth*
34 **2007**, *309* (2), 121–127. <https://doi.org/10.1016/j.jcrysgro.2007.09.025>.
35
36
37
38
39
40 (32) Wang, X.; Aroonyadet, N.; Zhang, Y.; Mecklenburg, M.; Fang, X.; Chen, H.; Goo, E.;
41 Zhou, C. Aligned Epitaxial SnO₂ Nanowires on Sapphire: Growth and Device Applications. *Nano*
42 *Lett.* **2014**, *14* (6), 3014–3022. <https://doi.org/10.1021/nl404289z>.
43
44
45
46
47 (33) Rafique, S.; Han, L.; Zhao, H. Synthesis of Wide Bandgap Ga₂O₃ (E_g ~ 4.6–4.7 eV) Thin
48 Films on Sapphire by Low Pressure Chemical Vapor Deposition. *Phys. Status Solidi A* **2016**, *213*
49
50 (4), 1002–1009. <https://doi.org/10.1002/pssa.201532711>.
51
52
53
54
55
56
57
58
59
60

1
2
3 (34) Yamashita, Y.; Honda, K.; Yagi, T.; Jia, J.; Taketoshi, N.; Shigesato, Y. Thermal
4 Conductivity of Hetero-Epitaxial ZnO Thin Films on c- and r-Plane Sapphire Substrates:
5 Thickness and Grain Size Effect. *J. Appl. Phys.* **2019**, *125* (3), 035101.
6
7 <https://doi.org/10.1063/1.5055266>.

8
9
10
11
12 (35) Perrière, J.; Hebert C.; Nistor M.; Millon E.; Ganem J.J.; Jedrecy N. Zn_{1-x}Fe_xO films: from
13 transparent Fe-diluted ZnO wurtzite to magnetic Zn diluted Fe₃O₄ spinel. *J. Mat. Chem.* **2015**, *3*,
14
15 11239-11249.
16
17 <https://doi.org/10.1039/C5TC02090E>

18
19
20
21
22 (36) Sano, T.; Tsuji, M.; Tamaura, Y. Effect of Foreign cations of Zn (II) or Mn (II) ion in FeO-
23 wustite on its disproportionation reaction below 575°C. *Solid State Ionics* **1997**, *104*, 311-317.
24
25 [https://doi.org/10.1016/S0167-2738\(97\)00432-3](https://doi.org/10.1016/S0167-2738(97)00432-3)

26
27
28
29 (37) Versluijs, J. J.; Bari, M. A.; Coey, J. M. D. Magnetoresistance of Half-Metallic Oxide
30 Nanocontacts. *Phys. Rev. Lett.* **2001**, *87* (2), 026601.
31
32 <https://doi.org/10.1103/PhysRevLett.87.026601>.

33
34
35 (38) Hu, G.; Suzuki, Y. Negative Spin Polarization of Fe₃O₄ in Magnetite/Manganite-Based
36 Junctions. *Phys. Rev. Lett.* **2002**, *89* (27), 276601.
37
38 <https://doi.org/10.1103/PhysRevLett.89.276601>.

39
40
41 (39) Seki, M.; Takahashi, M.; Adachi, M.; Yamahara, H.; Tabata, H. Fabrication and
42 Characterization of Wüstite-Based Epitaxial Thin Films: P-Type Wide-Gap Oxide
43
44
45
46
47
48
49
50
51
52
53
54
55
56
57
58
59
60

1
2
3 Semiconductors Composed of Abundant Elements. *Appl. Phys. Lett.* **2014**, *105* (11), 112105.

4
5 <https://doi.org/10.1063/1.4896316>.

6
7
8 (40) Fuji, Y.; Hara, M.; Yuasa, H.; Murakami, S.; Fukuzawa, H. Enhancement of
9
10 Magnetoresistance by Ultra-Thin Zn Wüstite Layer. *Appl. Phys. Lett.* **2011**, *99* (13), 132103.

11
12 <https://doi.org/10.1063/1.3644470>.

13
14
15 (41) Narayan, J.; Dovidenko, K.; Sharma, A. K.; Oktyabrsky, S. Defects and Interfaces in
16
17 Epitaxial ZnO/ α -Al₂O₃ and AlN/ZnO/ α -Al₂O₃ Heterostructures. *J. Appl. Phys.* **1998**, *84* (5),

18
19 2597–2601. <https://doi.org/10.1063/1.368440>.

20
21
22 (42) Narayan, J.; Pant, P.; Chugh, A.; Choi, H.; Fan, J. C. C. Characteristics of Nucleation Layer
23
24 and Epitaxy in GaN/Sapphire Heterostructures. *J. Appl. Phys.* **2006**, *99* (5), 054313.

25
26 <https://doi.org/10.1063/1.2178660>.

27
28
29 (43) Seiler, W.; Nistor, M.; Hebert, C.; Perrière, J. Epitaxial Undoped Indium Oxide Thin Films:
30
31 Structural and Physical Properties. *Sol. Energy Mater. Sol. Cells* **2013**, *116*, 34–42.

32
33 <https://doi.org/10.1016/j.solmat.2013.04.002>.

34
35
36 (44) Sbaï, N.; Perrière, J.; Seiler, W.; Millon, E. Epitaxial Growth of Titanium Oxide Thin Films
37
38 on C-Cut and α -Cut Sapphire Substrates. *Surf. Sci.* **2007**, *601* (23), 5649–5658.

39
40 <https://doi.org/10.1016/j.susc.2007.09.019>.

41
42
43 (45) Hoghooghi, B.; Raj, R. Controlled Epitaxial Nucleation of Nickel Oxide on
44
45 Microfabricated Magnesium Oxide Substrates in a CVD Process. *J. Am. Ceram. Soc.* **1996**, *79* (4),

46
47 1025–1033. <https://doi.org/10.1111/j.1151-2916.1996.tb08543.x>.

48
49
50 (46) Mozhaev, P. B.; Mozhaeva, J. E.; Khoryushin, A. V.; Bindslev Hansen, J.; Jacobsen, C. S.;
51
52 Bdikin, I. K.; Kotelyanskii, I. M.; Luzanov, V. A. Three-Dimensional Graphoepitaxial Growth of

1
2
3 Oxide Films by Pulsed Laser Deposition. *Phys. Rev. Mater.* **2018**, *2* (10), 103401.
4
5 <https://doi.org/10.1103/PhysRevMaterials.2.103401>.

6
7 (47) Noguera, C. Polar Oxide Surfaces. *J. Phys. Condens. Matter* **2000**, *12* (31), R367.
8
9 <https://doi.org/10.1088/0953-8984/12/31/201>.

10
11 (48) Chu, Y.-H. Van Der Waals Oxide Heteroepitaxy. *Npj Quantum Mater.* **2017**, *2* (1), 67.
12
13 <https://doi.org/10.1038/s41535-017-0069-9>.

14
15 (49) Utama, M. I. B.; Zhang, Q.; Jia, S.; Li, D.; Wang, J.; Xiong, Q. Epitaxial II–VI Tripod
16
17 Nanocrystals: A Generalization of van Der Waals Epitaxy for Nonplanar Polytypic
18
19 Nanoarchitectures. *ACS Nano* **2012**, *6* (3), 2281–2288. <https://doi.org/10.1021/nn204344z>.

20
21 (50) Ke, S.; Xie, J.; Chen, C.; Lin, P.; Zeng, X.; Shu, L.; Fei, L.; Wang, Y.; Ye, M.; Wang, D.
22
23 Van Der Waals Epitaxy of Al-Doped ZnO Film on Mica as a Flexible Transparent Heater with
24
25 Ultrafast Thermal Response. *Appl. Phys. Lett.* **2018**, *112* (3), 031905.
26
27 <https://doi.org/10.1063/1.5010358>.

28
29 (51) Maréchal, C.; Lacaze, E.; Seiler, W.; Perrière, J. Growth Mechanisms of Laser Deposited
30
31 BiSrCaCuO Films on MgO Substrates. *Phys. C Supercond.* **1998**, *294* (1–2), 23–32.
32
33 [https://doi.org/10.1016/S0921-4534\(97\)01735-8](https://doi.org/10.1016/S0921-4534(97)01735-8).

34
35 (52) Portier, X.; Hebert, C.; Briand, E.; Perrière, J.; Millon, E.; Cachoncinlle, C.; Nistor, M.;
36
37 Jedrecy, N. Microstructure of Nanocomposite Wurtzite-Spinel (Fe:ZnO)-(Zn:Fe₃O₄) Epitaxial
38
39 Films. *Mater. Chem. Phys.* **2019**, *229*, 130–138.
40
41 <https://doi.org/10.1016/j.matchemphys.2019.02.089>.

42
43 (53) Hebert, C. Zn_xFe_{1-x}O_{1+δ} Nanocomposite Films: Wurtzite and Spinel Phases, Sorbonne
44
45 University, Paris, 2017.

- 1
2
3 (54) Le Boulbar, E.; Millon, E.; Mathias, J.; Boulmer-Leborgne, C.; Nistor, M.; Gherendi, F.;
4 Sbaï, N.; Quoirin, J. B. Pure and Nb-Doped TiO_{1.5} Films Grown by Pulsed-Laser Deposition for
5
6 Transparent p–n Homojunctions. *E-MRS 2010 Spring Meet. Symp. R Laser Process. Diagn. Micro*
7
8 *Nano Appl.* **2011**, 257 (12), 5380–5383. <https://doi.org/10.1016/j.apsusc.2010.10.149>.
9
10
11 (55) Chaoui, N.; Millon, E.; Muller, J. F.; Ecker, P.; Bieck, W.; Migeon, H. N. On the Role of
12
13 Ambient Oxygen in the Formation of Lead Titanate Pulsed Laser Deposition Thin Films. *Appl.*
14
15 *Surf. Sci.* **1999**, 138–139, 256–260. [https://doi.org/10.1016/S0169-4332\(98\)00403-6](https://doi.org/10.1016/S0169-4332(98)00403-6).
16
17
18 (56) Chaoui, N.; Millon, E.; Muller, J. F.; Ecker, P.; Bieck, W.; Migeon, H. N. Perovskite Lead
19
20 Titanate PLD Thin Films: Study of Oxygen Incorporation by ¹⁸O Tracing Technique. *Mater.*
21
22 *Chem. Phys.* **1999**, 59 (2), 114–119. [https://doi.org/10.1016/S0254-0584\(99\)00051-6](https://doi.org/10.1016/S0254-0584(99)00051-6).
23
24
25 (57) Nistor, M.; Petitmangin, A.; Hebert, C.; Seiler, W. Nanocomposite Oxide Thin Films
26
27 Grown by Pulsed Energy Beam Deposition. *E-MRS 2010 Spring Meet. Symp. R Laser Process.*
28
29 *Diagn. Micro Nano Appl.* **2011**, 257 (12), 5337–5340.
30
31 <https://doi.org/10.1016/j.apsusc.2010.11.139>.
32
33
34 (58) Clatot, J.; Nistor, M.; Rougier, A. Influence of Si Concentration on Electrical and Optical
35
36 Properties of Room Temperature ZnO:Si Thin Films. *Thin Solid Films* **2013**, 531, 197–202.
37
38 <https://doi.org/10.1016/j.tsf.2013.01.046>.
39
40
41 (59) Rodriguez-Carvajal, J. Recent Developments of the Program Fullprof. *Commission on*
42
43 *Powder Diffraction (IUCr). Newsletter.* 2001st ed. pp 12–19.
44
45
46 (60) Calvert, C. C.; Brown, A.; Brydson, R. Determination of the Local Chemistry of Iron in
47
48 Inorganic and Organic Materials. *Electron Energy Loss Spectrosc. Electron Microsc.* **2005**, 143
49
50 (2), 173–187. <https://doi.org/10.1016/j.elspec.2004.03.012>.
51
52
53
54
55
56
57
58
59
60

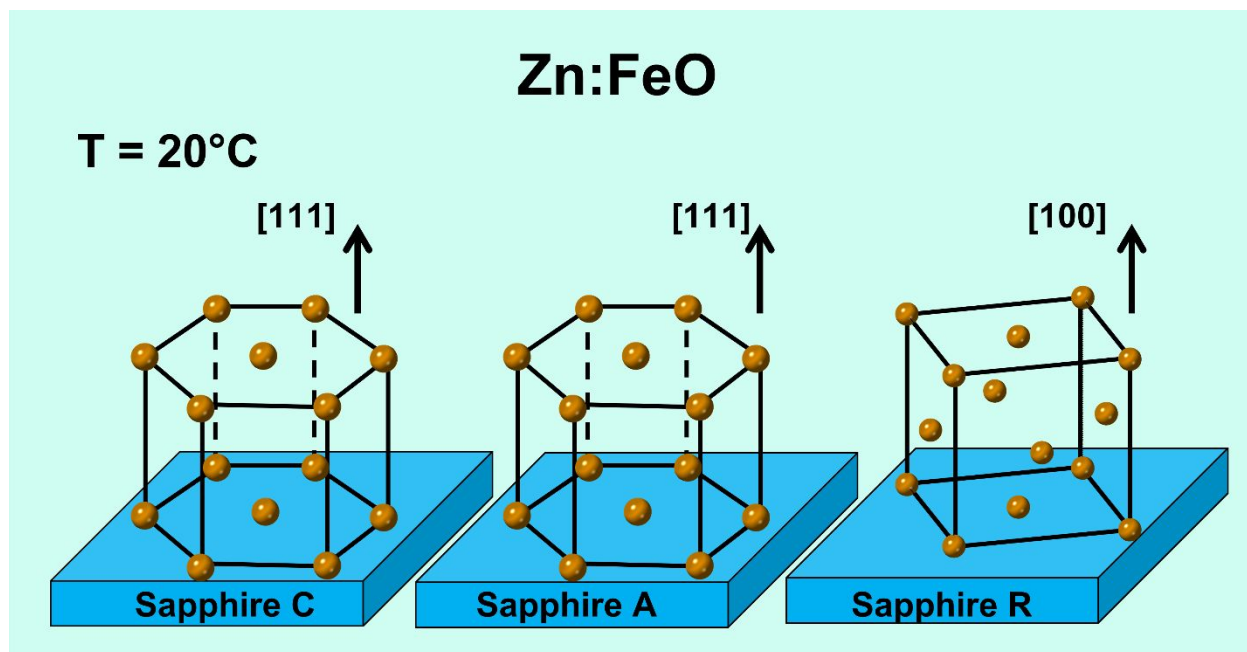
- 1
2
3 (61) Chen, J.; Deng, H.; Ji, H.; Tian, Y. Effect of Substrate Microstructure on the Misorientation
4 of A-Plane ZnO Film Investigated Using x-Ray Diffraction. *J. Vac. Sci. Technol. A* **2011**, *29* (3),
5
6 03A116. <https://doi.org/10.1116/1.3573670>.
7
8
9
10 (62) Savvides, N.; Thorley, A.; Gnanarajan, S.; Katsaros, A. Epitaxial Growth of Cerium Oxide
11 Thin Film Buffer Layers Deposited by d.c. Magnetron Sputtering. *Thin Solid Films* **2001**, *388* (1),
12 177–182. [https://doi.org/10.1016/S0040-6090\(01\)00839-2](https://doi.org/10.1016/S0040-6090(01)00839-2).
13
14
15
16 (63) Wang, F.; Müller, S.; Wördenweber, R. Large-Area Epitaxial MgO Buffer Layers on
17 Sapphire Substrates for Y-Ba-Cu-O Dilm Deposition. *Thin Solid Films* **1993**, *232* (2), 232–236.
18
19 [https://doi.org/10.1016/0040-6090\(93\)90014-G](https://doi.org/10.1016/0040-6090(93)90014-G).
20
21
22
23 (64) P A Stampe; M Bullock; W P Tucker; Robin J Kennedy. Growth of MgO Thin Films on
24 M-, A-, C- and R-Plane Sapphire by Laser Ablation. *J. Phys. Appl. Phys.* **1999**, *32* (15), 1778.
25
26 <https://doi.org/10.1088/0022-3727/32/15/304>.
27
28
29
30 (65) Malikov, I. V.; Berezin, V. A.; Fomin, L. A.; Chernykh, A. V. Epitaxial Fe₃O₄ Films
31 Grown on R-Plane Sapphire by Pulsed Laser Deposition. *Inorg. Mater.* **2020**, *56* (2), 164–171.
32
33 <https://doi.org/10.1134/S0020168520020120>.
34
35
36
37 (66) Zheleva, T.; Jagannadham, K.; Narayan, J. Epitaxial-Growth in Large-Lattice-Mismatch
38 Systems. *J. Appl. Phys.* **1994**, *75* (2), 860–871. <https://doi.org/10.1063/1.356440>.
39
40
41
42 (67) Bick, D. S.; Sharath, S. U.; Hoffman, I.; Major, M.; Kurian, J.; Alff, L. (001) and (111)
43 Single-Oriented Highly Epitaxial CeO₂ Thin Films on r-Cut Sapphire Substrates. *J. Electron.*
44 *Mater.* **2015**, *44* (8), 2930–2938. <https://doi.org/10.1007/s11664-015-3728-2>.
45
46
47
48 (68) Zhao, P.; Ito, A.; Tu, R.; Goto, T. High-Speed Epitaxial Growth of (100)-Oriented CeO₂
49 Film on r-Cut Sapphire by Laser Chemical Vapor Deposition. *Surf. Coat. Technol.* **2011**, *205* (16),
50 4079–4082. <https://doi.org/10.1016/j.surfcoat.2011.02.062>.
51
52
53
54
55
56
57
58
59
60

1
2
3 (69) Yamamoto, S.; Sugimoto, M.; Koshikawa, H.; Hakoda, T.; Yamaki, T. Orientational
4 Control of CeO₂ Films on Sapphire Substrates Grown by Magnetron Sputtering. *18th Int. Conf.*
5
6 *Cryst. Growth Epitaxy ICCGE-18* **2017**, *468*, 262–267.
7
8 <https://doi.org/10.1016/j.jcrysgro.2016.12.038>.
9
10
11
12
13
14
15
16
17
18
19
20
21
22
23
24
25
26
27
28
29
30
31
32
33
34
35
36
37
38
39
40
41
42
43
44
45
46
47
48
49
50
51
52
53
54
55
56
57
58
59
60

"For Table of Contents Use Only"

Room temperature epitaxial growth of Zn-doped iron oxide films on c-, a- and r-cut sapphire substrates

Valérie Demange, Xavier Portier, Sophie Ollivier, Mathieu Pasturel, Thierry Roisnel, Maryline Guilloux-Viry, Christian Hebert, Magdalena Nistor, Christophe Cachoncinlle, Eric Millon, Jacques Perrière



Synopsis: Room-temperature epitaxial growth of Zn doped FeO wüstite thin films on c-cut, a-cut and r-cut sapphire substrates

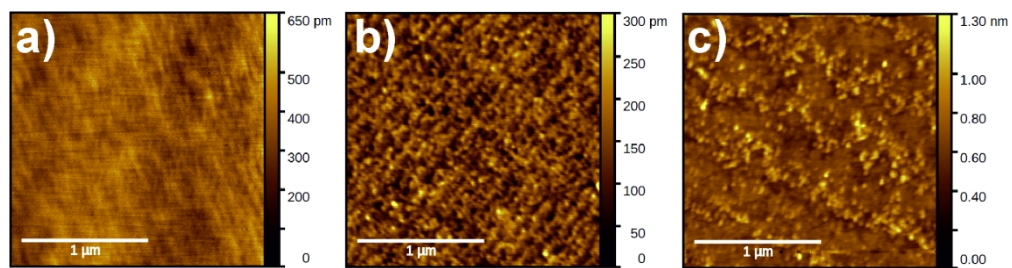


Figure 1. AFM image of c-cut, a-cut and r-cut sapphire substrates without any annealing before the PLD growth.

181x47mm (300 x 300 DPI)

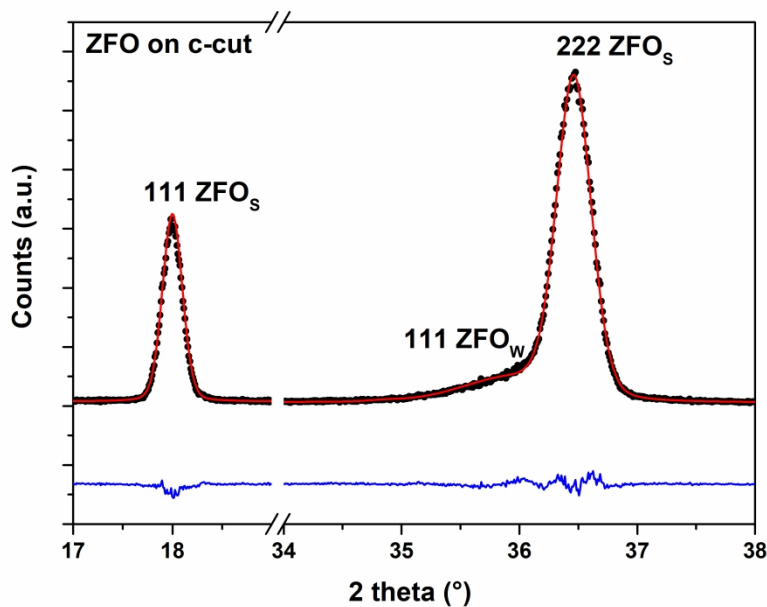


Figure 2. Experimental θ - 2θ XRD pattern (black symbols) of the ZFO film grown on c-cut sapphire substrate showing a peak at about 18° corresponding to the 111 Bragg reflection of the spinel phase and a broad peak around 36° corresponding to the 111 reflection of wüstite and the 222 reflection of spinel phases, respectively. This pattern has been refined using the Le Bail method and calculated and difference patterns are shown as red and blue lines, respectively.

288x201mm (300 x 300 DPI)

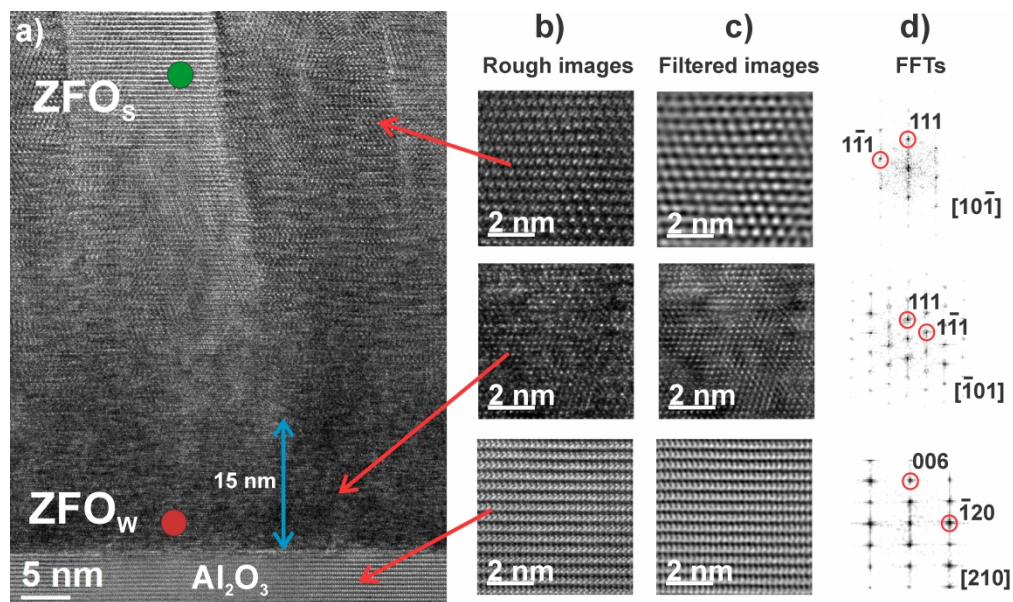


Figure 3. a) HREM image of a cross section of a ZFO film on c-cut sapphire substrate showing a thin region of ZFO_W at the bottom of the film; b) and c) are enlarged regions of the different parts of the film and the Al₂O₃ sapphire substrate corresponding to rough and filtered images respectively; d) FFTs of the previous mentioned images leading to the identification of the structures.

385x229mm (300 x 300 DPI)

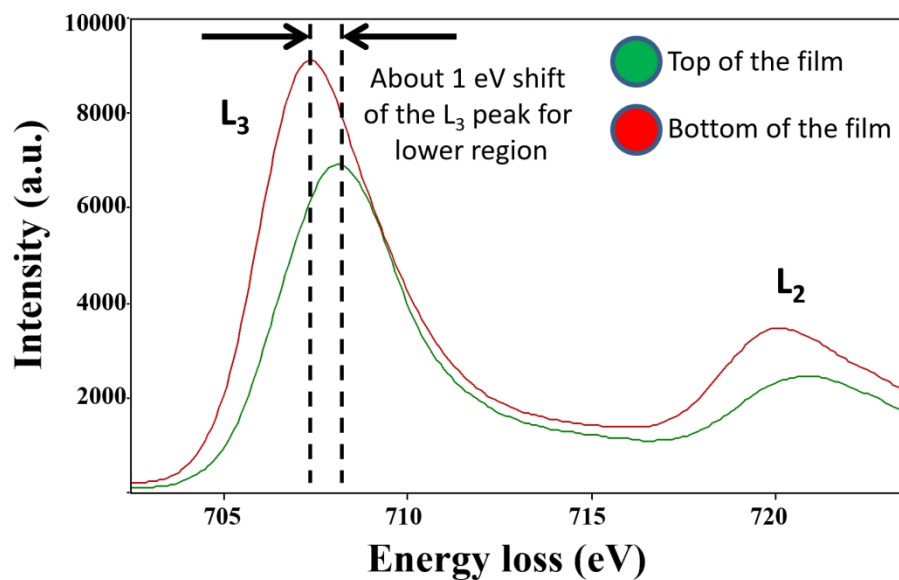


Figure 4. EELS spectra of the L₃ and L₂ energy thresholds of Fe. A 1 eV shift of the L₃ peak confirms the lowering of the valence state of Fe and thus the presence of wüstite at the bottom of the film.

141x90mm (330 x 330 DPI)

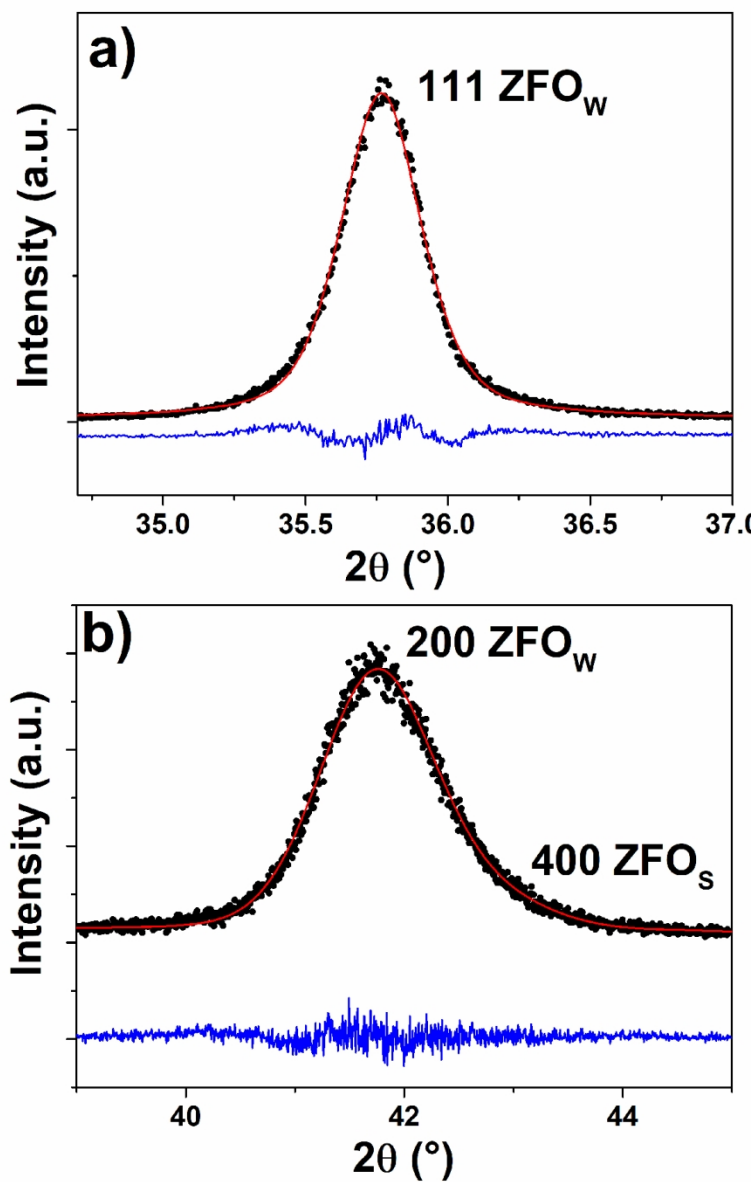
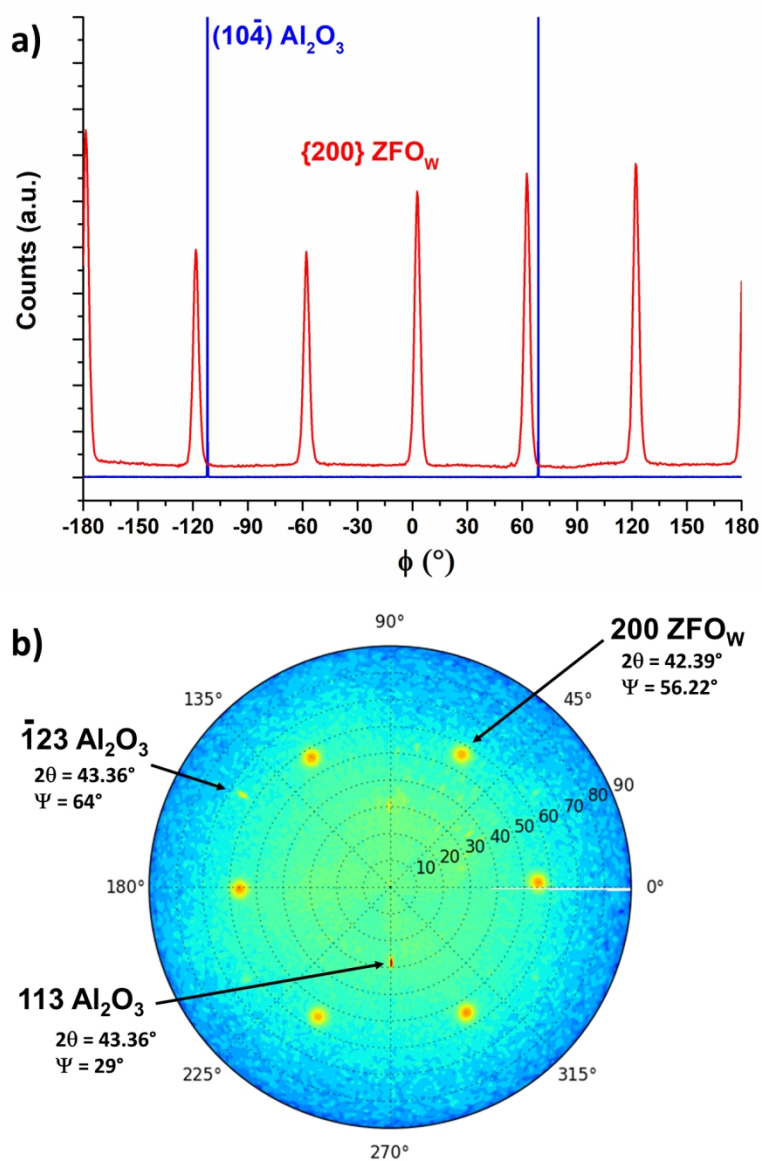


Figure 5. Le Bail refined θ - 2θ XRD patterns of ZFO films grown on a-cut (a) and r-cut (b) sapphire substrates. Black symbols display the experimental data, red lines represent the theoretical patterns and blue curves show the difference between them.

102x161mm (300 x 300 DPI)



45 Figure 6. a) Phi-scan of the $\{200\}$ planes of the (111) ZFOw film (red) and of the (10-4) planes of the a-cut
46 sapphire substrate (blue). b) Pole figure of the $\{200\}$ planes of the (111) ZFOw film showing 6 poles.

47 230x346mm (150 x 150 DPI)

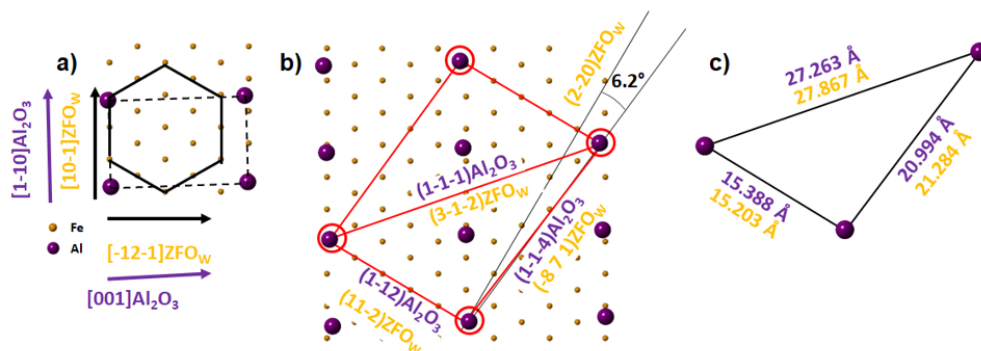
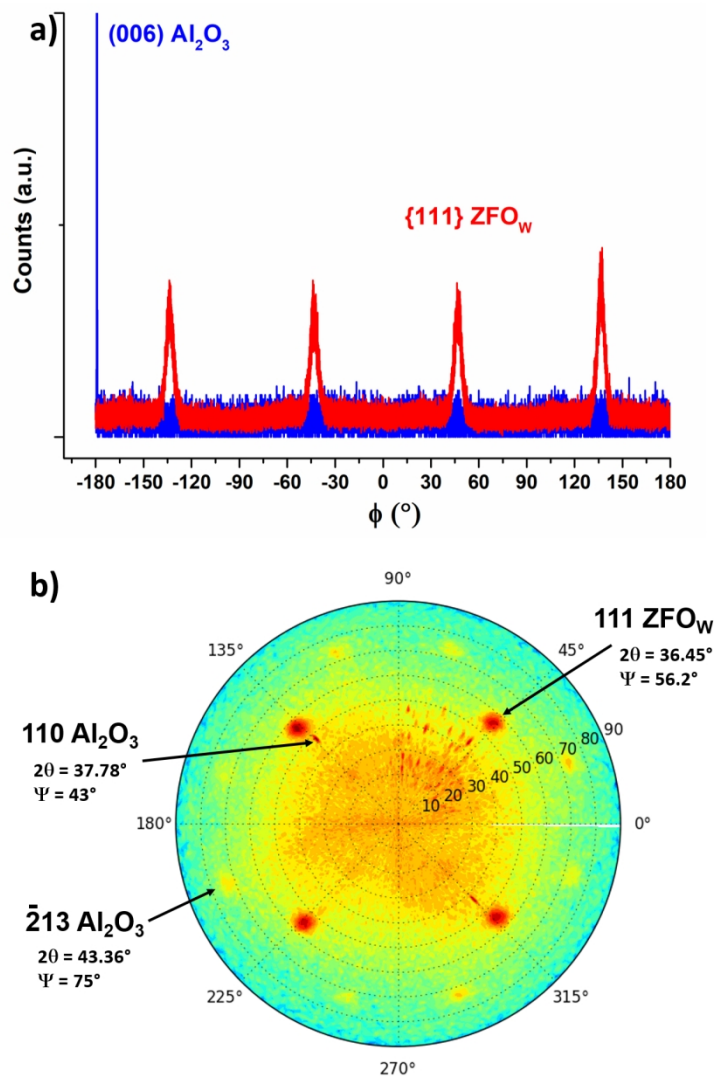


Figure 7: a) Scheme of the epitaxy of (111) ZFO_W grown on the a-cut sapphire substrate, determined by phi-scans measurement. b) Scheme of the domain matching epitaxy of (111) ZFO_W grown on the a-cut sapphire substrate, showing the site coincidences between the two lattices. The 6.2° rotation between the (2-20) ZFO_W plane and the (1-1-4) sapphire plane highlighted in the phi-scans is shown. c) Interatomic distances of the two lattices reported on the scheme.

254x93mm (96 x 96 DPI)



45 Figure 8: a) Phi-scan of the $\{111\}$ planes of the (100) ZFO_w film (red) and of the (006) plane of the r-cut
46 sapphire substrate (blue). b) Pole figure of the $\{111\}$ planes of the (100) ZFO_w film showing 4 poles.

47 251x376mm (150 x 150 DPI)

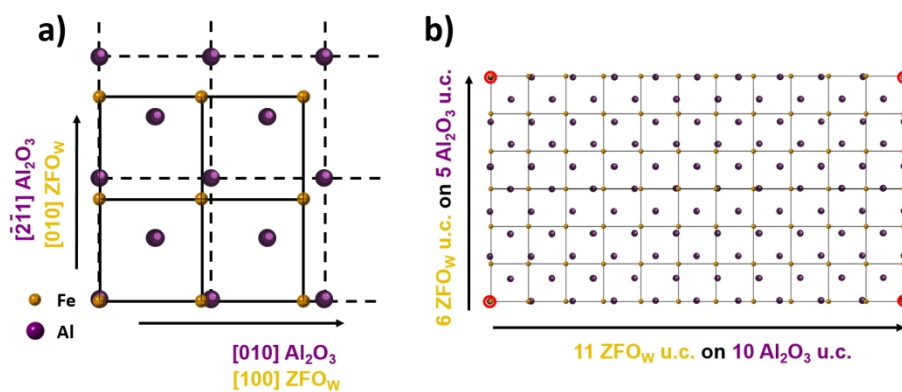


Figure 9: a) Scheme of the epitaxy of (100) ZFO_w grown on r-cut sapphire substrate. b) Scheme of domain matching epitaxy of (100) ZFO_w grown on r-cut sapphire substrate.

309x138mm (150 x 150 DPI)